Synthesis, Magnetism and Photoluminescence of Mn Doped AlN Nanowires

Qiushi Wang (wang_jiu_jiu@foxmail.com)
Bohai University
Li Yang
Bohai University
Junhong Li
Bohai University
Huadong Yang
Bohai University
Zhenbao Feng
Liaocheng University
Zhu Ge
Dalian Minzu University: Dalian Nationalities University
Jian Zhang
Beihua University
Yao Lin
Beihua University
Xuejiao Wang
Beihua University
Chuang Wang
Bohai University
Ying Fu
Songshan Lake Materials Laboratory
Cailong Liu
Liaocheng University

Research Article

Keywords: AlN, Mn doped, Ferromagnetic, Photoluminescence

Posted Date: August 3rd, 2021

DOI: https://doi.org/10.21203/rs.3.rs-763003/v1

Abstract

Manganese doped aluminum nitride (AlN:Mn) nanowires were fabricated by direct nitridation of Al and Mn mixed powders. The as-synthesized AlN:Mn nanowires were characterized by X-ray diffraction, Raman, energy-dispersive X-ray spectroscopy, X-ray photoelectron spectroscopy, scanning and transmission electron microscopy. The measurements reveal the successful incorporation of Mn^{2+} ions into AlN nanowires. The magnetic and optical properties of the AlN:Mn nanowires were studied using vibrating sample magnetometer and photoluminescence spectroscopy. The AlN:Mn nanowires exhibit room temperature ferromagnetic behavior and a red emission band centered at 597 nm corresponding to the $^4T_1(^4G)$-$^6A_1(^6S)$ transition of Mn^{2+}. The abnormal thermal quenching behavior and long afterglow feature are investigated through the temperature dependent emission and the afterglow spectrum. The thermoluminescence curve shows that AlN: Mn nanowires have a wide trap distribution, which leads to the abnormal thermal quenching behavior and persistent luminescence. Multifunctional AlN:Mn nanowires with magnetic and luminescence properties are expected to be used in spintronic and optoelectronic nanodevices.

1. Introduction

During the past decades, one-dimensional (1D) nanostructures have attracted much attention because of their unique physical properties and potential applications in the nanodevices and nanocomposites [1, 2]. Aluminum nitride (AlN) is a kind of III–V semiconductor with many excellent properties such as widest direct band-gap (6.2 eV), high thermal conductivity, good mechanical strength, high piezoelectric response, and negative electron affinity [3]. Thus, the controllable 1D AlN nanostructures were successfully prepared by different methods, which have desirable applications in the field of short wavelength light emitting and field emission devices [4–6].

Because doping is an ideal way to improve electrical, optical and magnetic properties of AlN semiconductor, more and more studies on transition metal and rare earth doped AlN are carried out [7–12]. Especially, Mn doped AlN (AlN:Mn) has aroused a lot of interest because of its potential applications in diluted magnetic semiconductors (DMS) and red light-emitter. For example, Frazier et al. have prepared AlN:Mn thin films with different Mn contents through gas-source molecular beam epitaxy [13]. Yang et al. have fabricated AlN:Mn nanowires via a simple vapor phase deposition method [14]. Li et al. have synthesized AlN:Mn polycrystalline powders by solid-state reaction [15]. The room temperature ferromagnetism was observed in AlN:Mn thin films, nanowires and polycrystalline powders as described above, indicating that ferromagnetism is an intrinsic property of AlN:Mn. On the other hand, the AlN:Mn thin films with a single emission band around 600 nm has been prepared by chemical vapor deposition [16]. Wang et al. have prepared Mn^{2+} doped AlN phosphors with a strong red emission through solid-state reaction method, which has great potential in full-color field emission display [17]. Later, Xu et al. have studied the afterglow feature of AlN:Mn, indicating its brightness is 0.65 mcd/m^2 after stopping ultraviolet (UV) radiation for 60 minutes, and duration upon 0.32 mcd/m^2 can reach more than 110

minutes [18]. Lei. et al. have also prepared AlN:Mn red phosphors through a solid-state reaction, which can be used as white light-emitting diodes [19]. Although AlN:Mn films and bulk materials and their properties have been extensively explored, there are very few reports on the synthesis of 1D AlN:Mn nanostructures, due to the limited equilibrium solubility of Mn in AlN semiconductor and the intrinsic difficulties in doping nanocrystal. Thus, the preparation and characterization of AlN:Mn nanowires is a challenging work, which is helpful to explore their properties and applications. Also, compared with thin films and bulk materials, nanowires have many advantages, such as nanoscale size, low dimension, and single crystal, which are potential nanoscale building blocks for electronic and optoelectronic devices. If the DMS nanowires exhibit robust magnetism, they will be important for application in spintronic nanodevices using electronic spin as an additional degree of freedom. Therefore, we decided to explore the possibility of synthesizing AlN:Mn nanowires, which may be a potential magnetic and optical multifunctional nanomaterial.

In previous works, we have used improved arc discharge method for the preparation of multifunctional AlN nanostructures doped with a series of rare earth elements [12, 20–25]. In this paper, AlN:Mn nanowires have been synthesized by direct nitridation of Al and Mn mixed powders using similar method. Various experimental methods are used to characterize the as-prepared nanowires. A promising magnetic and optical properties of the AlN:Mn nanowires is demonstrated. The abnormal thermal quenching behavior and long afterglow feature AlN:Mn nanowires of are also explained. This work provides a new opportunity to design AlN based nanomaterials for optoelectronic and magnetic functionalities on a single chip.

2. Experimental Section

The sample preparation was carried out in a direct current (DC) discharge plasma setup described previously [26, 27]. The anode was Al and Mn mixed powder, while the cathode was a tungsten needle. The Mn content in AlN:Mn nanowires was controlled by changing the molar ratio of Mn powder to Al powder. The chamber pressure was evacuated to less than 1 Pa, then the N_2 gas was introduced into chamber to 20 kPa. During the experimental process, the current and potential were maintained at 100 A and 25 V for 5 min, respectively. After being passivated in 40 kPa Ar for 24 h, the grey white powder was seen to get settled on the water-cooling wall.

The AlN:Mn nanowires thus synthesized was characterized by X-ray diffraction (XRD, Rigaku D/Max-A diffractometer), X-ray photoelectron spectroscopy (XPS, VG ESCA LAB MKII), Micro-Raman spectroscopy (JY-T800, excited with solid-state laser at 532 nm), scanning electron microscopy (SEM, HITACHI S-4800 microscope), energy dispersive X-ray spectroscopy (EDS), and high resolution transmission electron microscopy (HRTEM, JEM-2200FS). The magnetic measurements were studied using a vibrating sample magnetometer (VSM, Lake Shore 7400). The photoluminescence (PL) spectra and afterglow decay curve were obtained by an fluorescence spectrophotometer (Hitachi F-4600). The thermoluminescent (TL) curve was detected by a thermoluminescent dosimeter (FJ-427A, Beijing Nuclear Instrument Factory) with a heating rate of 1°C/s.

3. Results And Discussions

The chemical compositions of AlN nanowires with different Mn concentrations were measured by EDS. The at.% of Mn (*x*) is found to be 0.0, 0.4, 0.9, 1.3 and 2.3 in the samples, respectively. The XRD pattens of AlN nanowires doped with diverse concentrations of Mn ions (AlN: *x*Mn) are presented in Fig. 1 (a). For all samples, the diffraction peaks in patterns can be indexed as wurtzite-structured AlN (PDF card No. 08-0262). Under the resolution of XRD, no peak of impurity phase is detected. As show in Fig. 1 (b), with the increase of doping concentration, the (1 0 0), (0 0 2), and (1 0 1) peak positions shift towards lower angles, indicating lattice constant broadening due to the substitution of Al^{3+} (0.054 nm) by larger Mn^{2+} (0.067 nm).

Raman scattering is a powerful tool for detecting dopant incorporation, lattice defects and disorders. The Raman spectra of the as-prepared AlN:Mn nanowires are shown in Fig. 2. For AlN: 0.0%Mn nanowires, four Raman scattering peaks locating at 251, 612, 659 and 671 cm^{-1} are assigned to E_2(low), A_1(transverse optical (TO)), E_2(high) and E_1(TO) modes of the wurtzite AlN, respectively. A low-intensity and wide peak around 900 cm^{-1} is caused by the A_1(longitudinal optical (LO)) and E_1(LO) modes. With increasing of the Mn concentration in nanowires, the A_1 (TO), E_2 (high) and E_1(TO) peaks gradually broaden and move to lower frequencies due to increasing of defect concentration and disorders resulting from incorporation of Mn^{2+} ions. The results can further confirm that the Al ions are substituted by Mn ions in AlN nanowires.

The XPS measurement is used to determine the valence state of Mn in the AlN nanowires. The XPS spectrum of AlN: 0.9%Mn nanowires are performed in Fig. 3. The survey scan XPS spectrum in Fig. 3 (a) shows strong peaks for aluminum and nitrogen as expected, except for the C 1s peak from the reference and O 1s peak from absorbed gaseous. As shown in Fig. 3 (b) and (c), the Al 2p peak centered at 73.4 eV and N 1s peak centered at 396.8 eV are related to binding energy of aluminum and nitrogen in AlN, respectively. The Mn 2p XPS spectrum (Fig. 3(d)) displays two major peaks with binding energy values at 642.2 and 654.5 eV, corresponding to the Mn $2p_{3/2}$ and Mn $2p_{1/2}$ peaks, respectively. Between them, a peak at 647.6 eV corresponding to the shake-up satellite suggests the presence of Mn^{2+}. The results of XRD, EDS, Raman and XPS confirm the successful incorporation of Mn^{2+} ions into AlN nanowires.

The morphology of the as-synthesized AlN:0.9%Mn nanowires was performed using SEM, as shown in Fig. 4 (a), (b) and (c), revealing that the product consists of high-density nanowires with very high aspect ratio. The diameter of the nanowires ranges from 30 to 200 nm and the length extends to several micrometers. The chemical composition of nanowires is checked by the EDS analysis, as shown in Fig. 4(d). The composition analysis is clear that the contents of Mn in AlN nanowires are about 0.9%.

A typical TEM image of an AlN:0.9%Mn nanowire is given in Fig. 5(a), which clearly shows that the diameter of the nanowire is about 50 nm, which is the same as that observed by SEM. Figure 5(b) shows the HRTEM image recorded from the edge of the nanowire. The adjacent lattice spacing is about 0.25 nm, which is consistent with the (001) facet distance of hexagonal AlN, indicating that the nanowire grows

along [001] direction. In addition to this, many dark spots can be seen in the lattice, which are attributed to local lattice distortions and defects caused by the larger Mn^{2+} ions replacing Al^{3+} in the nanowires.

In recent years, the potential applications of AlN-based DMS in spintronics have attracted great interest. To explore the magnetism of AlN:Mn nanowires, the magnetic measurements of AlN: Mn nanowires with different Mn concentrations are carried out at room temperature using VSM. Figure 6 shows the corresponding magnetic hysteresis (M-H) curves for 0.0, 0.4, 0.9, 1.3 and 2.3 at% Mn doped AlN nanowires. All AlN:Mn samples exhibit well-defined hysteresis loops and ferromagnetic behaviors. The saturation magnetization (M_s) and coercivity values (H_c) of AlN:xMn nanowires are shown in Table 1. According to the results of XRD, Raman, XPS and HRTEM, it can be confirmed that the Mn^{2+} ions are successfully doped into AlN nanowires without changing wurtzite structure, and excluded the possibility of other impurities. Thus, the observed room temperature ferromagnetism is the intrinsic properties of AlN:Mn nanowires.

Table 1
saturation magnetization (M_s) and coercivity values (H_c) of AlN:xMn nanowires.

Mn ratio (at. %)	M_s (emu/g)	H_c (Oe)
0.0	0.015	35.4
0.4	0.032	40.0
0.9	0.045	48.9
1.3	0.058	77.0
2.3	0.050	83.4

Up to now, the ferromagnetic origin of DMSs is still confusing. There are two most prevalent mechanisms of ferromagnetism in DMS: the carrier-mediated model and the bound magnetic polaron (BMP) model [28, 29]. Because AlN has a high resistance at room temperature, the carrier-mediated model is not suitable for explaining the ferromagnetic properties of the AlN:Mn nanowires and the BMP model is the preferred mechanism for AlN: Mn nanowires [30]. Based on BMP model, the magnetism for semiconductors is very sensitive to the defects such as dopants, anion or cation vacancies and interstitials. Mn has the $3d^5 4s^2$ valence configuration. According to Hund's rule, there are five unpaired 3d electrons with same spin direction, which may contribute to magnetic ordering. However, the possibility of ferromagnetic coupling is very small when the concentration of Mn^{2+} is low in the doped AlN nanowires. In previous literatures, the doping of large functional ions in AlN can easily lead to high Al or N vacancies, because of large size mismatch [31, 32]. Also, the presence of high Al or N vacancies in the AlN:Mn nanowires are revealed by HRTEM, which trap electrons and mediate the magnetic spin of Mn^{2+}, leads to the delocalized magnetic moments and long-range coupling of the BMPs. Therefore, the ferromagnetism of AlN:Mn nanowires may be due to BMPs produced by the interactions between the trapped electrons in Al or N vacancies and the magnetic spins of Mn^{2+} ions.

On increase Mn dopant ion concentration, the H_c increase gradually, which is related to the increase of Al or N vacancies in the nanowires. The increase in H_c values with increase doping concentration is similar to previous report for Sc doped AlN nanowires [33]. Meanwhile, it is noticed that the M_s is enhanced with the increase of Mn content (approximately up to 1.3%), and then decreases. This decrease in M_s is due to the fact that higher dopant ion concentrations result in shorter distances between the doped atoms, thus strengthening the antiferromagnetic interactions at the expense of ferromagnetic ordering [29, 34, 35]. Therefore, the Mn contents in AlN nanowires may exist a critical value. Below this value, M_s increases with increasing Mn concentration, and above this value, M_s decreases. In brief, the magnetic properties of AlN: Mn nanowires can be tuned by controlling the doping concentration of Mn.

Figure 7 (a) shows the PL and PL excitation (PLE) spectra of the AlN:0.9% nanowires. Under excitation at 266 nm, the AlN:0.9%Mn nanowires show an intense red emission band with a maximum at 597 nm, which corresponds to intra-atomic transition of Mn^{2+} from the excited state $^4T_1(^4G)$ to the ground state $^6A_1(^6S)$. As indicated in the inset of Fig. 7 (a), this bright red emission can be clearly seen by the naked eye under UV lamp (254 nm) irradiation. The full width at half-maximum of the emission band is about 39 nm, indicating luminescence of AlN:Mn nanowires have a high color purity. The PLE spectrum, monitored with 597 nm, shows a wide excitation peak with a maximum at 266 nm, which is associated with the defects of nitrogen substituted by O^{2-} in AlN lattice. Figure 7(b) shows the high resolution PLE spectrum in the wavelength range between 350 and 550 nm. In this range, the PLE spectrum consists of several weak peaks at 400, 455, 489, 520, and 548 nm corresponding to the spin and parity forbidden d-d transitions of Mn^{2+} from the ground state $^6A_1(^6S)$ to the excited state $^4E(^4D)$, $^4T_2(^4D)$, ($^4A_1(^4G)$, $^4E(^4G)$), $^4T_2(^4G)$ and $^4T_1(^4G)$ [17]. The valency of Mn ions in AlN remains controversial, because Mn^{4+} also exhibits red emission in the 560–670 nm range. Also, the ionic radius of Mn^{4+} (0.053 nm) is closer to Al^{3+} (0.054 nm) than Mn^{2+} (0.067 nm), suggesting Mn^{4+} is more easily doped into AlN lattice. However, the Mn^{4+} ions usually produce line emissions. Therefore, the successful doping of Mn^{2+} in AlN nanowires is also evident from the luminescence spectrum.

In order to study the effect of the Mn content on the optical properties, PL measurements were performed for AlN nanowires with Mn doping concentration ranging from 0.0 to 2.3%, as shown in Fig. 8. With increase of Mn^{2+} content, the emission intensity increases rapidly, reaches the maximum at 0.9%, and then decreases again at higher doping levels. The deterioration of the emission signal is usually attributed to concentration quenching caused by nonradiative energy transfer between adjacent doped Mn^{2+} ions.

The PL decay curves of AlN:*x*Mn nanowires monitored at 597 nm and excited at 266 nm are displayed in Fig. 9. The decay curves are well fitted by using the following double-exponential relationship:

$$I(t) = I_1 \exp\left(-\frac{t}{\tau_1}\right) + I_2 \exp\left(-\frac{t}{\tau_2}\right) \quad (1)$$

where I means the luminescence intensity, I_1 and I_2 represent constants, t stands for the time, τ_1 and τ_2 are decay times for exponential components. The detailed fitting parameters and lifetime values of AlN:xMn nanowires calculated by Eq. (1) are listed in Table 2. As with other Mn^{2+} doped materials, the lifetime is in the range of milliseconds [36]. It is well known that the PL intensity is related to the lifetime of the luminescent center and the radiation velocity [37]. For the same luminescent center, the radiation velocity can be supposed to constant (the amount of radiation photons in a specific period). Therefore, a stronger luminescence intensity corresponds to a longer fluorescence lifetime.

Table 2
Fitting parameters of different decay curves for AlN:xMn nanowires (with x = 0.0%, 0.4%, 0.9%, 1.3% and 2.3%).

Mn ratio (at. %)	I_1	τ_1(ms)	I_2	τ_2(ms)	t(ms)
0.0	10172.64	0.41	2314.08	2.61	1.71
0.4	9989.51	0.48	2873.16	2.77	1.91
0.9	8134.32	0.64	4815.46	2.76	2.16
1.3	9603.02	0.40	2765.95	2.74	1.96
2.3	10126.27	0.39	2150.14	2.66	1.73

The thermal stability of light-emitting materials is a key index to evaluate the potential application of the final devices, because it has an impact on the different characteristics of the device. Thus, it is necessary to elucidate the thermal stability of light-emitting materials according to the relationship between intensity and temperature. Figure 10 (a) and (b) presents the temperature dependent PL emission spectra and corresponding relative integrated intensity trend for AlN:0.9%Mn nanowires, respectively. It is important to note that the emission intensity of Mn^{2+} transition, initially increase slightly (until the temperature reached 353 K), and then gradually drops. When the temperature is below the 413 K, the emission intensity is still higher than initial value at 293 K. In general, an increasing of temperature can increase the population of higher vibration levels, the density of phonons and the probability of non-radiative transfer (energy migration to defects), leading to the emission intensity gradually drops. Here, the AlN:Mn nanowires exhibit an abnormal thermal quenching behavior, which should be related to the traps in AlN band gap. The detail of reason will be discussed later.

Figure 11 shows the afterglow decay curves of the AlN:0.9%Mn nanowires after irradiation by a 254 nm UV lamp for 3 min. The decay curve can be successfully fitted by Eq. (1), and the fitting results are summarized in Table 3. Apparently, the decay curve consists of a rapid attenuation process at first (τ_1) and then a slow decay process (τ_2). Due to the presence of the significant slow decay component (τ_2), the long afterglow features can last more than 30 min with brightness $\geq$ 0.32 mcd/m^2 in the darkroom. The observed afterglow feature of AlN:Mn nanowires can significantly save power compared with traditional LEDs, which paves the way for further dealing with severe environmental and energy problems.

Table 3
Simulated results for the afterglow curves of AlN:0.9%Mn nanowires

	I_1	τ_1(s)	I_2	τ_2(s)
value	247.19	18.40	173.58	123.26

It is considered that the existence of traps is the main reason for the abnormal thermal quenching behavior and afterglow performance. To further verify the presence of traps, the TL curve of AlN:0.9%Mn nanowires is shown in Fig. 12 (a). The TL curve gives an asymmetric shape and a wide temperature region from 300 to 620 K, suggesting a wide trap distribution. However, because the incorporation of larger-size Mn^{2+} ions into AlN lattice results in the coexistence and complexity of different defects, it's very difficult to discriminate and assign or calculate exact trap depths. Through calculations and experiments, N vacancies (V_N) with multiple charge states is generally considered to be formed shallow energy level at 0.12-1.0 eV below the conduction band (CB), and V_{Al} level located at 1.2–2.7 eV above the valence band (VB) [38, 39]. Oxygen impurities are another essential defects, and easy to incorporate into AlN:Mn^{2+} lattice for change balance. In general, oxygen impurities are located at N position to form separated oxygen point defects (O_N) and complex defects with Al vacancies (O_N-V_{Al}). The O_N energy level is at around 1.9 eV below the CB, and O_N-V_{Al} complex level is at around 1.2 eV above the VB [40, 41]. Figure 12 (b) exhibits a mechanism diagram for the abnormal thermal behavior and afterglow process. The strong excitation band centered at 266 nm (Fig. 7 (a)), is attributed to the excitation from the O_N-V_{Al} level to its excited state level (process ①). After UV light irradiation (process ②), most of the excitation energy related to the excited carriers (electrons or holes) will be directly transferred to the luminescence center Mn^{2+} (process ③), followed by the $^4T_1(^4G)$-$^6A_1(^6S)$ emission as the immediate luminescence (process ④). However, when some electrons transition into the CB and then are captured by V_N or O_N levels and the holes are captured by V_{Al} or O_N-V_{Al} levels, instead of returning to ground state (progress ⑤). After removing the UV light source, with the thermal disturbances at proper temperature, electrons and holes trapped by the defect levels will be gradually released, transferred to the luminescence center Mn^{2+} (process ⑥), and then emit as long afterglow (process ⑦). For thermal quenching process, as the sample is heated to proper temperature, the “stored” electrons in the defect levels can be excited to the excited level (process ⑧) and finally return to ground state. The higher temperature, the more electrons are excited through process ⑤ and ⑧ to process ⑥. Meanwhile, the higher temperature results in greater energy loss of the electrons in the relaxation process, due to the enhanced nonradiative transition, leading to the decrease of electrons in process ⑥ from process ⑤. Thus, the thermal quenching behavior should be the coupling contribution by the above two effects. When the electrons excited from process ⑧ to process ⑥ is higher than that lost in the relaxation process, leading to the increase of emission intensity and the abnormal thermal quenching behavior.

4. Conclusions

In conclusion, we report on the ferromagnetic and luminescence properties of AlN:Mn nanowires synthesized through direct nitrification of Al and Mn powder in arc discharge plasma with N_2 as the working medium. XRD, Raman, XPS and EDS studies show that Mn^{2+} ions enter AlN nanowires as substituents. The M-H curves indicate that AlN: Mn nanowires exhibit room temperature ferromagnetism, which is due to the unpaired electrons in the 3d shell of Mn^{2+} ions and the formation of Al or N vacancies. Also, AlN: Mn^{2+} nanowires displays a strong red emission band around at 597 nm, attributed to the $^4T_1$-$^6A_1$ transition of Mn^{2+} ions. With the concentration of Mn^{2+} enhanced, the saturation magnetization and emission of AlN:Mn nanowires strengthen and then attenuate. The abnormal thermal quenching and afterglow phenomena are found due to the generated plentiful traps resulting in the incorporation of larger-size Mn^{2+} ions into AlN lattice, which is revealed by TL curves. As a result, AlN: Mn nanowires provided great opportunities for the development of novel spintronic and optoelectronic devices.

Declarations

Acknowledgements

This study is supported financially by the National Natural Science Foundation of China (Grant No. 11874174), the Natural Science Foundation of Liaoning Province, China (grant No.2019-ZD-0490), Foundation of Liaoning Province Education Administration, China (grant No. LQ2020009), the Introduction and Cultivation Plan of Youth Innovation Talents for Universities of Shandong Province, the Special Construction Project Fund for Shandong Province Taishan Scholars and National Undergraduate Training Program for Innovation and Entrepreneurship (Grant No.202010201018).

References

1. Z. Liu, J. Xu, D. Chen, G.Z. Shen, Flexible electronics based on inorganic nanowires,*Chemical Society Reviews* 2015, **44**: 161-192.
2. K.S. Ryu, L. Thomas, S.H. Yang, S. Parkin, Chiral spin torque at magnetic domain walls, *Nature Nanotechnology* 2013, **8**: 527-533.
3. Y. Taniyasu, M. Kasu, T. Makimoto, An aluminium nitride light-emitting diode with a wavelength of 210 nanometres, *Nature* 2006, **441**: 325-328.
4. J.H. He, R.S. Yang, Y.L. Chueh, L.J. Chou, L.J. Chen, Z.L. Wang, Aligned AlN nanorods with multi-tipped surfaces-Growth, field-emission, and cathodoluminescence properties, *Advanced Materials* 2006, **18**:650-654.
5. Kenry, K.T. Yong, S.F. Yu, AlN nanowires: synthesis, physical properties, and nanoelectronics applications, *Journal of Materials Science* 2012, **47**:5341-5360.
6. J. Zheng, Y. Yang, B. Yu, X.B. Song, X.G. Li, 0001 oriented aluminum nitride one-dimensional nanostructures: Synthesis, structure evolution, and electrical properties, *Acs Nano* 2008, **2**: 134-142.

7. Y.S. Xu, B.B. Yao, D. Liu, W.W. Lei, P.W. Zhu, Q.L. Cui, G.T. Zou, Room temperature ferromagnetism in new diluted magnetic semiconductor AlN:Mg nanowires, *Crystengcomm* 2013, **15**: 3271-3274.
8. A. Aghdaie, H. Haratizadeh, S.H. Mousavi, S.A.J. Mohammadi, P.W. de Oliveira, Effect of doping on structural and luminescence properties of AlN nanowires, *Ceramics International* 2015, **41**: 2917-2922.
9. H. Li, G.M. Cai, W.J. Wang, Room temperature luminescence and ferromagnetism of AlN:Fe,*Aip Advances* 2016, **6**: 065025.
10. M.R. Hauwiller, D. Stowe, T.B. Eldred, S. Mita, R. Collazo, Z. Sitar, J. LeBeau, Cathodoluminescence of silicon doped aluminum nitride with scanning transmission electron microscopy, *Apl Materials* 2020, **8**: 091110.
11. W.W. Lei, D. Liu, P.W. Zhu, X.H. Chen, Q. Zhao, G.H. Wen, Q.L. Cui, G.T. Zou, Ferromagnetic Sc-doped AlN sixfold-symmetrical hierarchical nanostructures, *Applied Physics Letters* 2009, **95**: 162501.
12. R.D. Cong, J.M. Wang, X.Y. Wang, Y.F. Zhang, W.B. Lu, W. Zhao, Q.S. Wang, X.Y. Liu, W. Yu, Ferromagnetic anisotropy in scandium-doped AlN hierarchical nanostructures, *Journal of Materials Science* 2020, **55**: 8325-8336.
13. R. Frazier, G. Thaler, M. Overberg, B. Gila, C.R. Abernathy, S.J. Pearton, Indication of hysteresis in AlMnN, *Applied Physics Letters* 2003, **83**: 1758-1760.
14. Y. Yang, Q. Zhao, X.Z. Zhang, Z.G. Liu, C.X. Zou, B. Shen, D.P. Yu, Mn-doped AlN nanowires with room temperature ferromagnetic ordering, *Applied Physics Letters* 2007, **90**: 092118.
15. H. Li, H.Q. Bao, B. Song, W.J. Wang, X.L. Chen, L.J. He, W.X. Yuan, Ferromagnetic properties of Mn-doped AlN, *Physica B-Condensed Matter* 2008, **403**: 4096-4099.
16. A. Sato, K. Azumada, T. Atsumori, K. Hara, Low-temperature metalorganic chemical vapor deposition of luminescent manganese-doped aluminum nitride films, *Applied Physics Letters* 2005, **87**: 021907.
17. X.J. Wang, R.J. Xie, B. Dierre, T. Takeda, T. Suehiro, N. Hirosaki, T. Sekiguchi, H.L. Li, Z. Sun, A novel and high brightness AlN:Mn^{2+} red phosphor for field emission displays, *Dalton Transactions* 2014, **43**: 6120-6127.
18. J. Xu, N.J. Cherepy, J. Ueda, S. Tanabe, Red persistent luminescence in rare earth-free AlN:Mn^{2+} phosphor, *Materials Letters* 2017, **206**: 175-177.
19. F.F. Lei, X. Lei, Z.T. Ye, N. Zhao, X.W. Yang, Z. Shi, H. Yang, Photoluminescent properties of AlN: Mn^{2+} phosphors, *Journal of Alloys and Compounds* 2018, **763**: 466-470.
20. Q.S. Wang, Y.H. Xie, J. Zhang, R.D. Cong, Synthesis, photoluminescence and ferromagnetic properties of pencil-like Y doped AlN microrods, *Ceramics International* 2017, **43**: 3319-3323.
21. Q.S. Wang, W.Z. Wu, J. Zhang, G. Zhu, R.D. Cong, Formation, photoluminescence and ferromagnetic characterization of Ce doped AlN hierarchical nanostructures, *Journal of Alloys and Compounds* 2019, **775**: 498-502.
22. Q.S. Wang, W.Z. Wu, W. Zhang, J. Zhang, G. Zhu, X.J. Wang, R.D. Cong, Tunable optical and magnetic properties of Tm-doped AlN nanostructures, *Journal of Magnetism and Magnetic Materials* 2019,

487: 165305.

23. Q.S. Wang, W.Z. Wu, K. Wang, H.L. Zheng, G. Zhu, J. Zhang, H. Cui, Q.L. Cui, High pressure photoluminescence properties and structural stability of Eu doped AlN nanowires synthesized via a direct nitridation strategy, *Journal of Alloys and Compounds* 2020, **823**.
24. Q.S. Wang, J.H. Li, J. Zhang, G. Zhu, H.L. Zheng, R.D. Cong, Novel self-assembled microstructures made from Dy doped AlN nanosheets: Formation mechanism, photoluminescence and magnetic properties, *Applied Surface Science* 2020, 527.
25. Q.S. Wang, J.H. Li, W. Zhang, H.L. Zheng, R.D. Cong, Synthesis, and photoluminescence and magnetic properties of Tb-doped AlN single-crystalline nanobelts, *Journal of Luminescence* 2021, **236**: 118089.
26. J. Zhang, H.Y. Zhu, X.X. Wu, H. Cui, D.M. Li, J.R. Jiang, C.X. Gao, Q.S. Wang, Q.L. Cui, Plasma-assisted synthesis and pressure-induced structural transition of single-crystalline *SnSe nanosheets, Nanoscale* 2015, **7**:10807-10816.
27. G. Zhu, W.Z. Wu, S.Y. Xin, J. Zhang, Q.S. Wang, Plasma-assisted synthesis of ZnSe hollow microspheres with strong red emission, *Journal of Luminescence* 2019, **206**: 33-38.
28. J.M.D. Coey, M. Venkatesan, C.B. Fitzgerald, Donor impurity band exchange in dilute ferromagnetic oxides, *Nature Materials* 2005, **4**:173-179.
29. J.T. Luo, Y.Z. Li, X.Y. Kang, F. Zeng, F. Pan, P. Fan, Z. Jiang, Y. Wang, Enhancement of room temperature ferromagnetism in Cu-doped AlN thin film by defect engineering, *Journal of Alloys and Compounds* 2014, **586**: 469-474.
30. A. Kaminski, S. Das Sarma, Polaron percolation in diluted magnetic semiconductors, *Physical Review Letters* 2002, **88**: 247202.
31. W.W. Lei, D. Liu, X. Chen, P.W. Zhu, Q.L. Cui, G.T. Zou, Ferromagnetic Properties of Y-Doped AlN Nanorods, *Journal of Physical Chemistry C* 2010, **114**: 15574-15577.
32. R. Ishikawa, A.R. Lupini, F. Oba, S.D. Findlay, N. Shibata, T. Taniguchi, K. Watanabe, H. Hayashi, T. Sakai, I. Tanaka, Y. Ikuhara, S.J. Pennycook, Atomic Structure of Luminescent Centers in High-Efficiency Ce-doped w-AlN Single Crystal, *Scientific Reports* 2014, **4**: 3778.
33. X.Y. Liu, J.S. Mi, B. Zhang, J. Zhang, Q.S. Wang, R.D. Cong, Dopant concentration dependent magnetism of Sc-doped AlN nanowires, *Journal of Alloys and Compounds* 2018, **731**: 1037-1043.
34. J. Xiong, P. Guo, F. Guo, X.L. Sun, H.S. Gu, Room temperature ferromagnetism in Mg-doped AlN semiconductor films, *Materials Letters* 2014, **117**: 276-278.
35. H.R. Hu, Z.G. Wu, W.B. Zhang, H.J. Li, R.F. Zhuo, D. Yan, J. Wang, P.X. Yan, Temperature-dependent growth, photoluminescence and ferromagnetic properties of co-doped AlN hexagonal nanostructures, *Materials Letters* 2015, **142**: 106-108.
36. C.H. Huang, T.W. Kuo, T.M. Chen, Novel red-emitting phosphor $Ca_9Y(PO_4)_7$:Ce^{3+}, Mn^{2+} with energy transfer for fluorescent lamp application, *Acs Applied Materials & Interfaces* 2010, **2**: 1395-1399.

37. Q. Dong, J. Cui, Y.B. Tian, J.J. Jia, F.L. Yang, F. Du, J.Q. Peng, X.Y. Ye, S.H. Yang, Enhanced narrow-band green-emission and thermal stability via the introduction of Mg^{2+} in ZnB_2O_4: Mn^{2+} phosphor, *Crystengcomm* 2019, **21**: 5947-5957.
38. K. Laaksonen, M.G. Ganchenkova, R.M. Nieminen, Vacancies in wurtzite GaN and AlN, *Journal of Physics-Condensed Matter* 2009, **21**: 015803.
39. H.R. Hu, Z.G. Wu, W.B. Zhang, H.J. Li, R.F. Zhuo, D. Yan, J. Wang, P.X. Yan, Effect of Mg doping on growth and photoluminescence of AlN hexagonal nanorods, *Journal of Alloys and Compounds* 2015, **624**: 241-246.
40. B. Berzina, L. Trinkler, J. Sils, K. Atobe, Luminescence mechanisms of oxygen-related defects in AlN, *Radiation Effects and Defects in Solids-Incorporating Plasma Science and Plasma Technology* 2002, **157**: 1089-1092.
41. R.A. Youngman, J.H. Harris, Luminescence studies of oxygen-related defects in aluminum nitride, *Journal of the American Ceramic Society* 1990, **73**: 3238-3246.

Figures

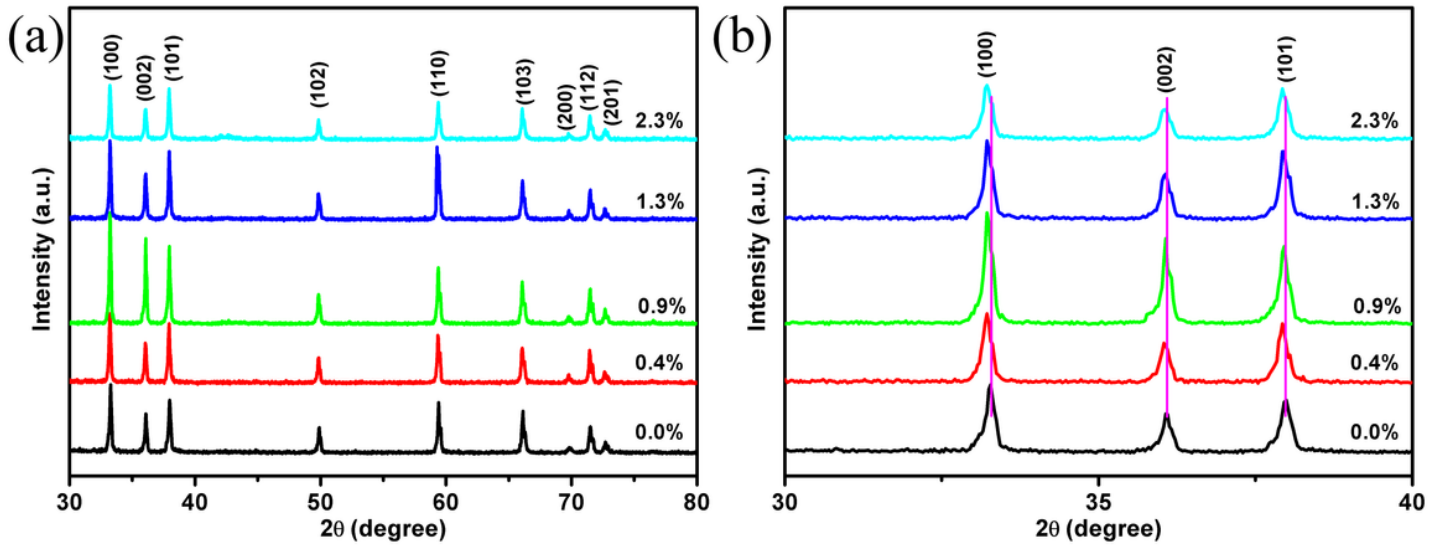

Figure 1

(a) XRD patterns of the AlN: xMn (x = 0.0 %, 0.4 %, 0.9 %, 1.3 % and 2.3 %) nanowires and (b) the enlargement of (100), (002) and (101) diffraction peaks for all samples.

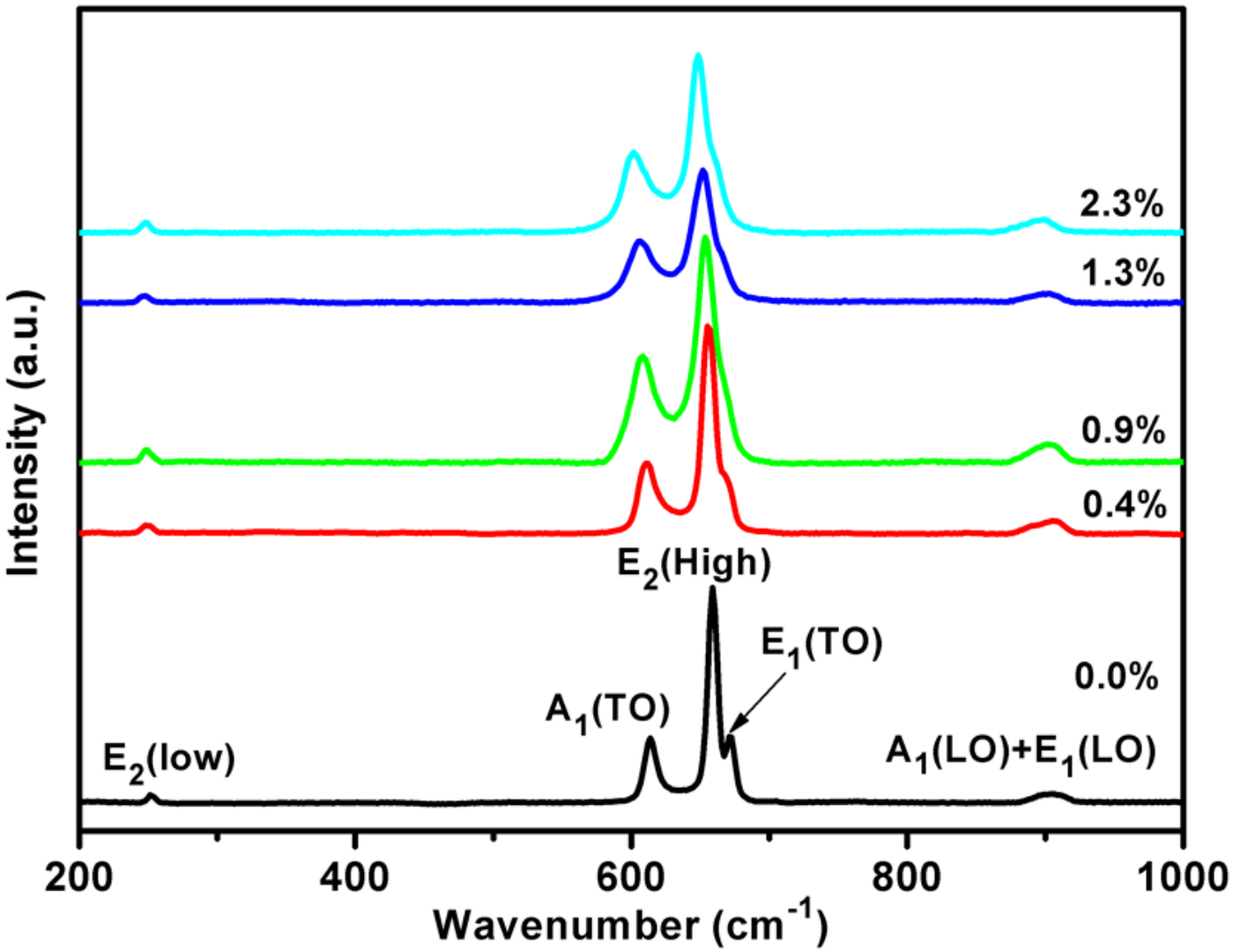

Figure 2

Raman spectra of the AlN: xMn nanowires with x = 0.0 %, 0.4 %, 0.9 %, 1.3 % and 2.3 %, respectively.

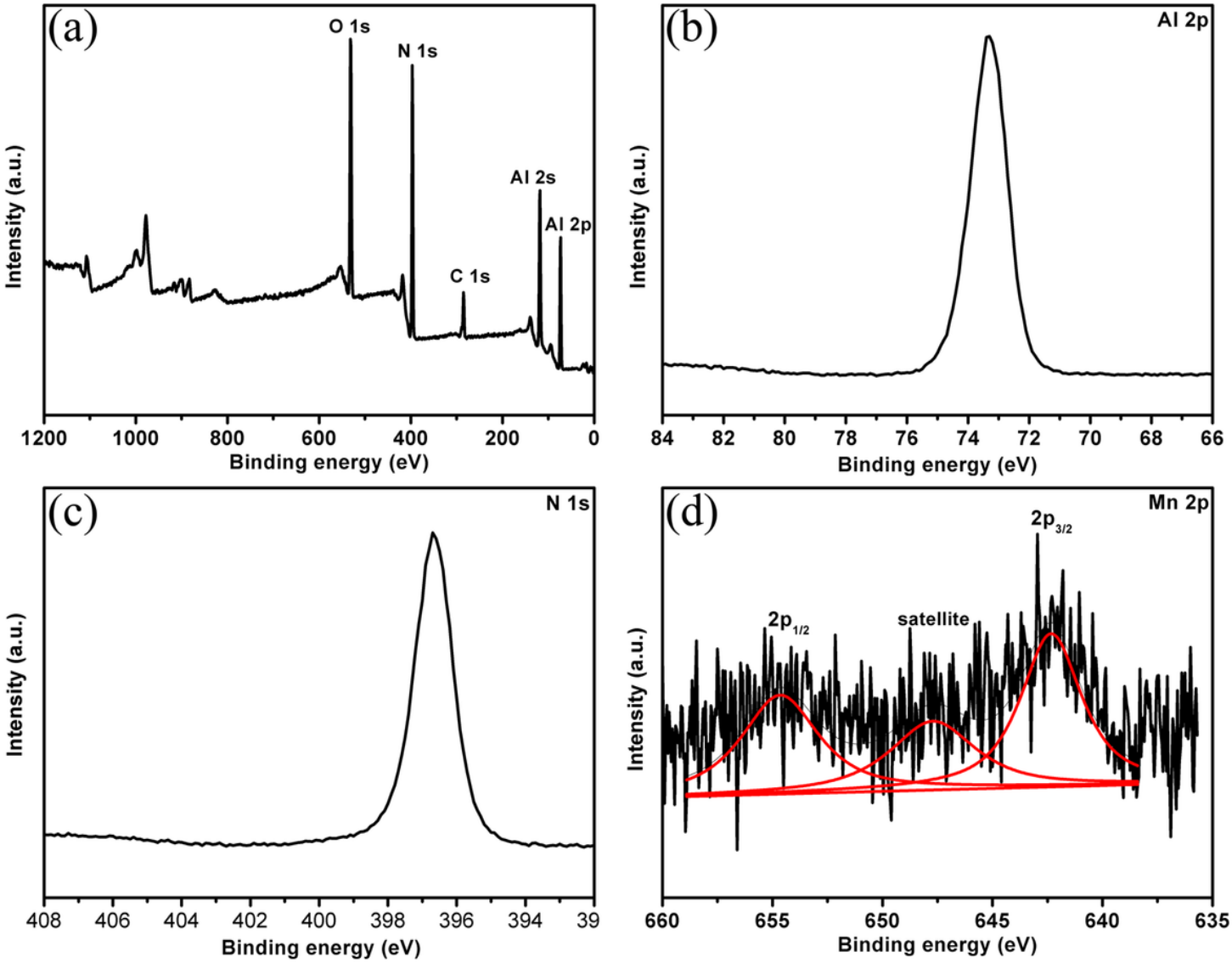

Figure 3

XPS spectra of AlN: 0.9 % Mn nanowires: (a) survey scan, (b) Al 2p, (c) N 1 s, and (d) Mn 2p core levels, respectively.

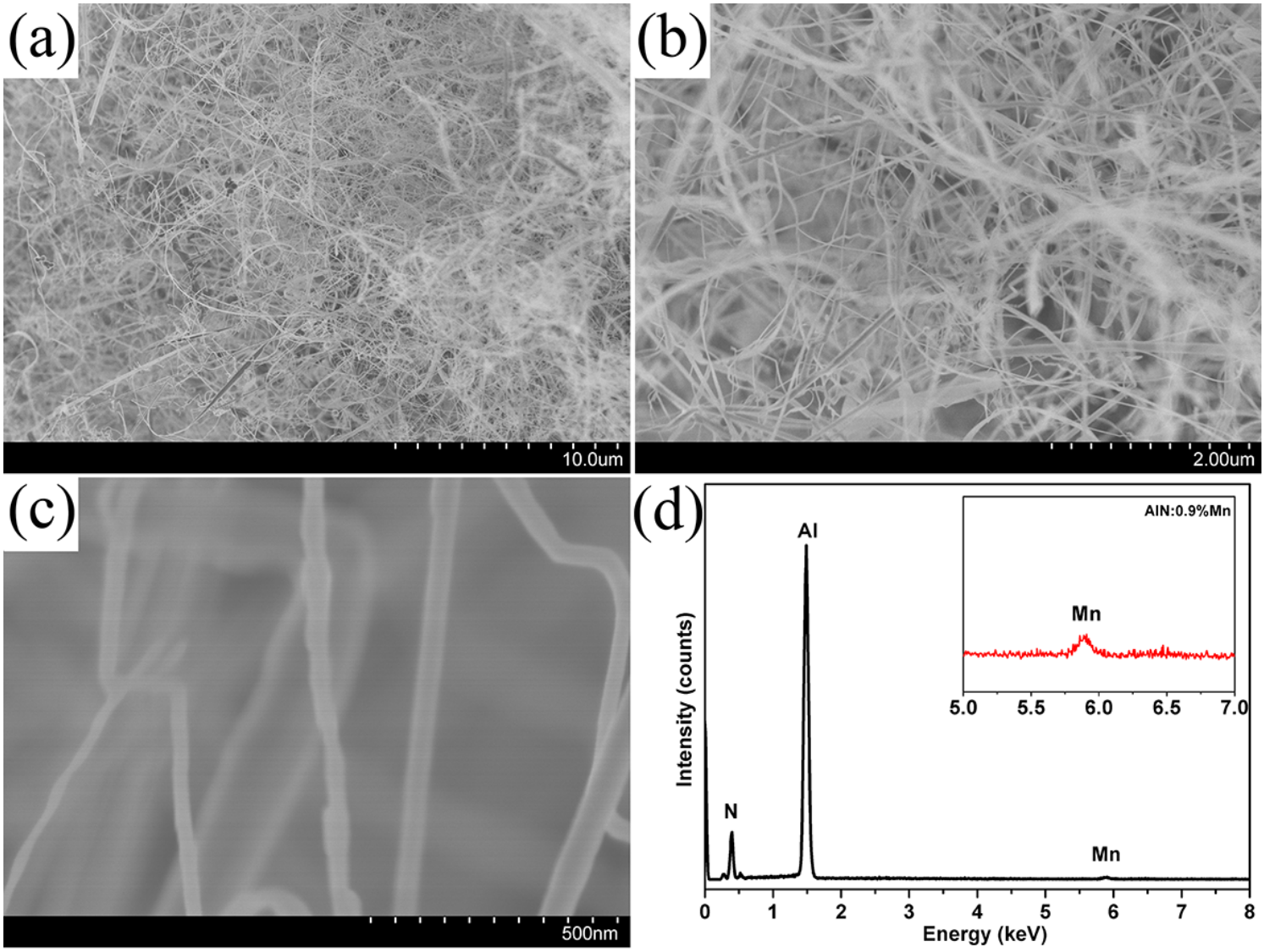

Figure 4

Low-(a, b) and high-(c) magnification SEM image and EDS spectrum (d) of the AlN: 0.9 % Mn nanowires.

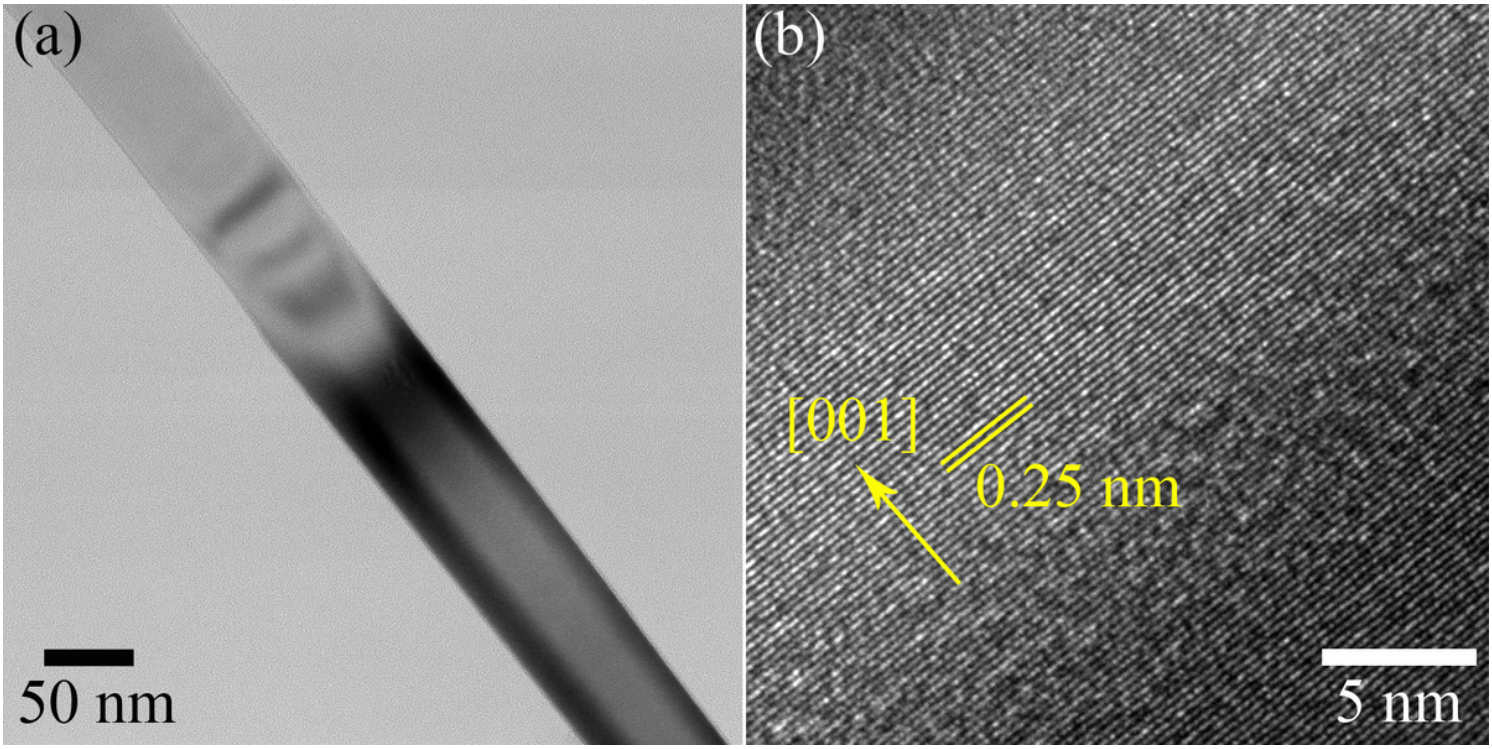

Figure 5

(a) TEM image and HRTEM lattice image of the typical AlN: 0.9 % nanowire.

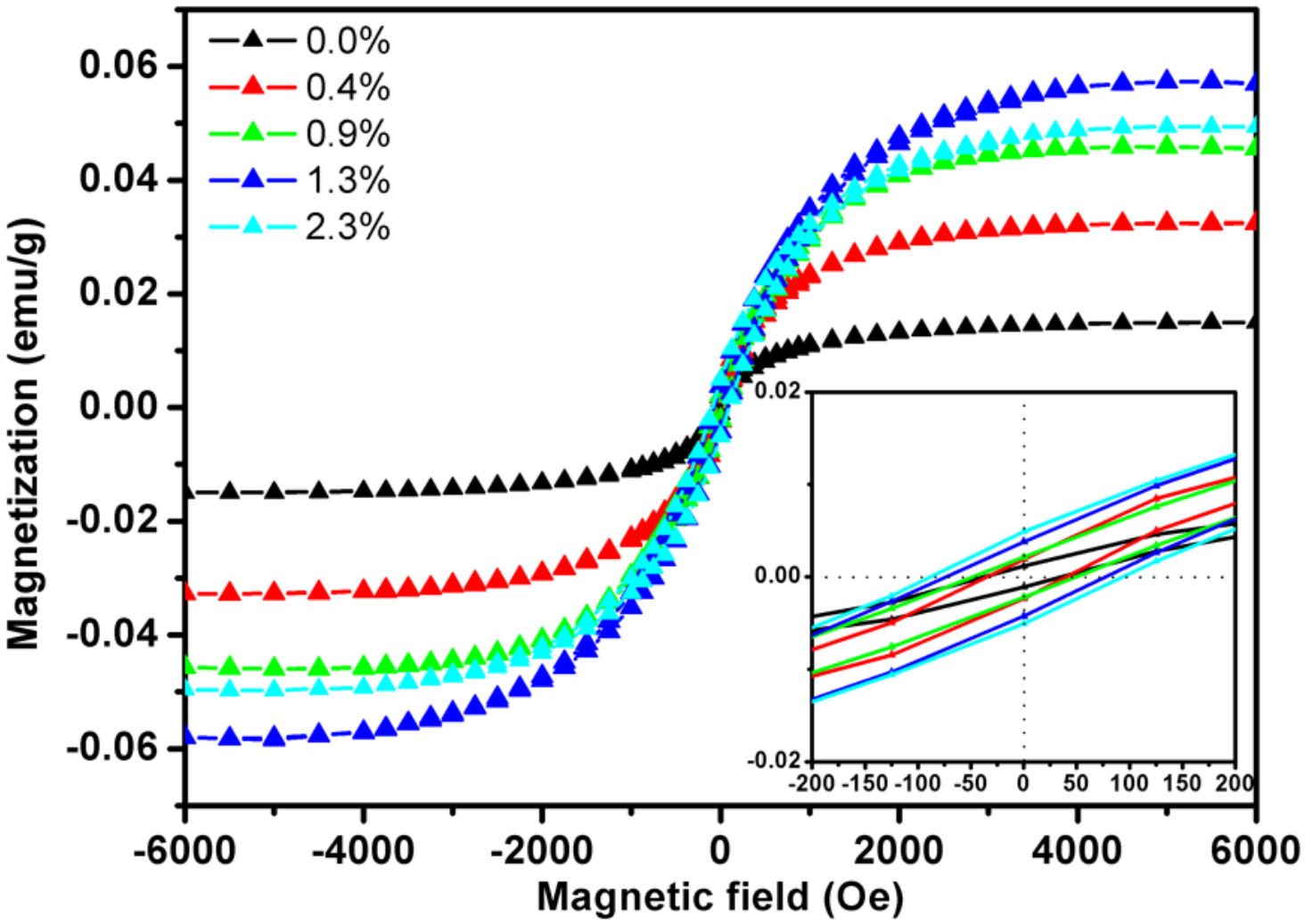

Figure 6

Magnetization hysteresis loops of the AlN: xMn nanowires (with x = 0.0 %, 0.4 %, 0.9 %, 1.3 % and 2.3 %) at room temperature, and the inset is the magnetization curves in low-field region.

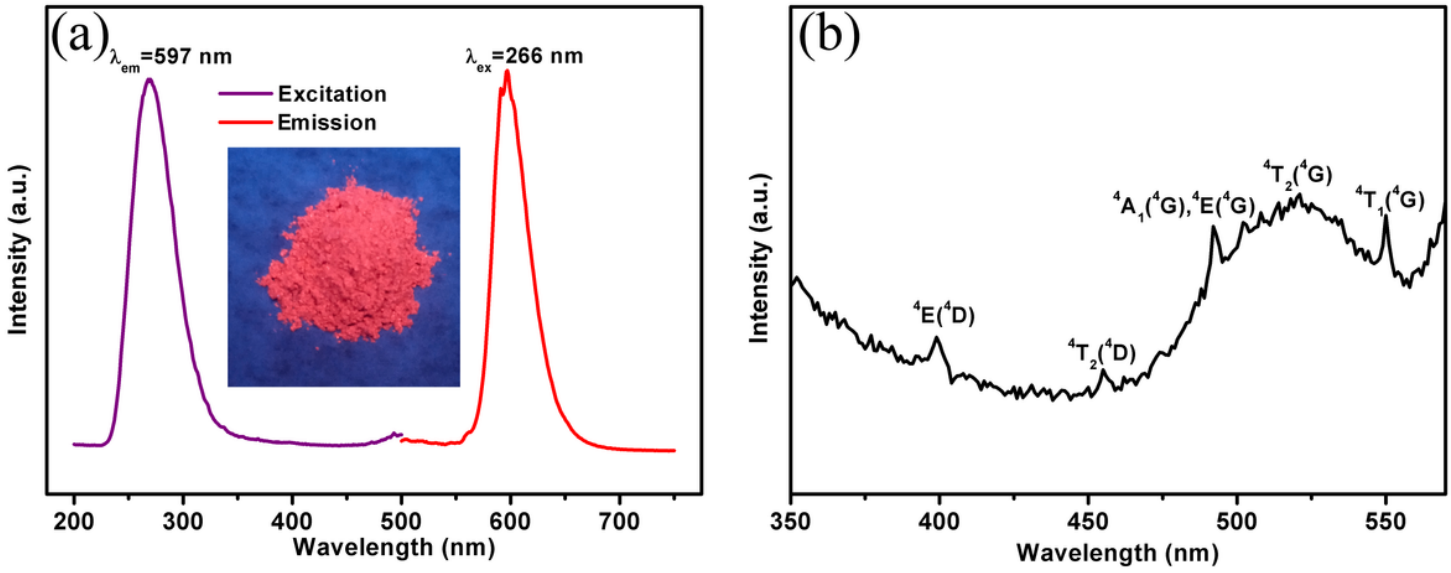

Figure 7

the PL excitation spectrum (monitoring emission wavelength λem =597 nm) and emission spectrum (under excitation wavelength λex= 266 nm) of AlN: 0.9 % Mn nanowires. The inset is a photograph of the AlN: 0.9 % Mn nanowires under UV lamp (254 nm) irradiation, (b) the enlarged excitation spectrum in the range of 350-550 nm.

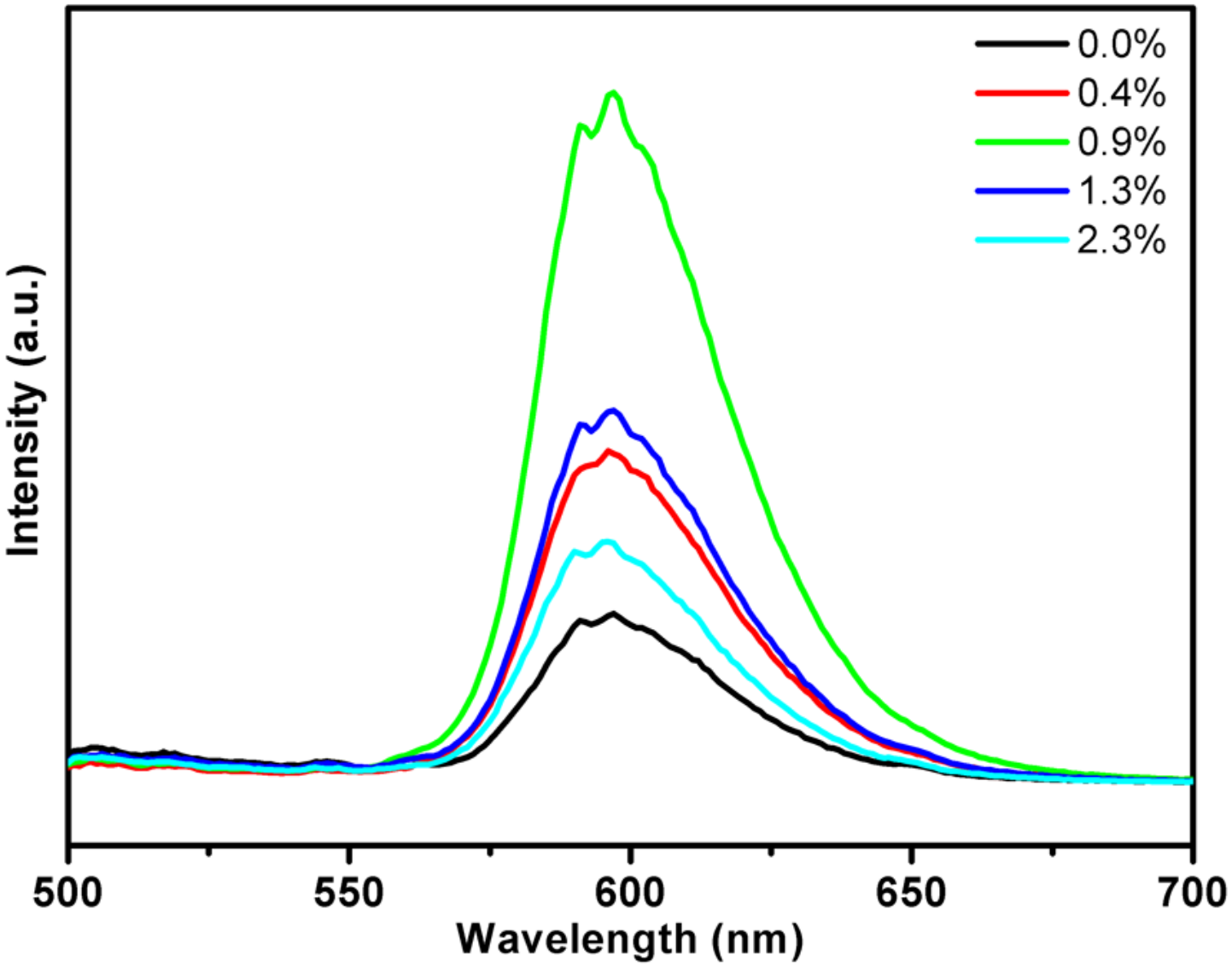

Figure 8

Emission spectra of AlN: xMn nanowires (with x = 0.0 %, 0.4 %, 0.9 %, 1.3 % and 2.3 %)

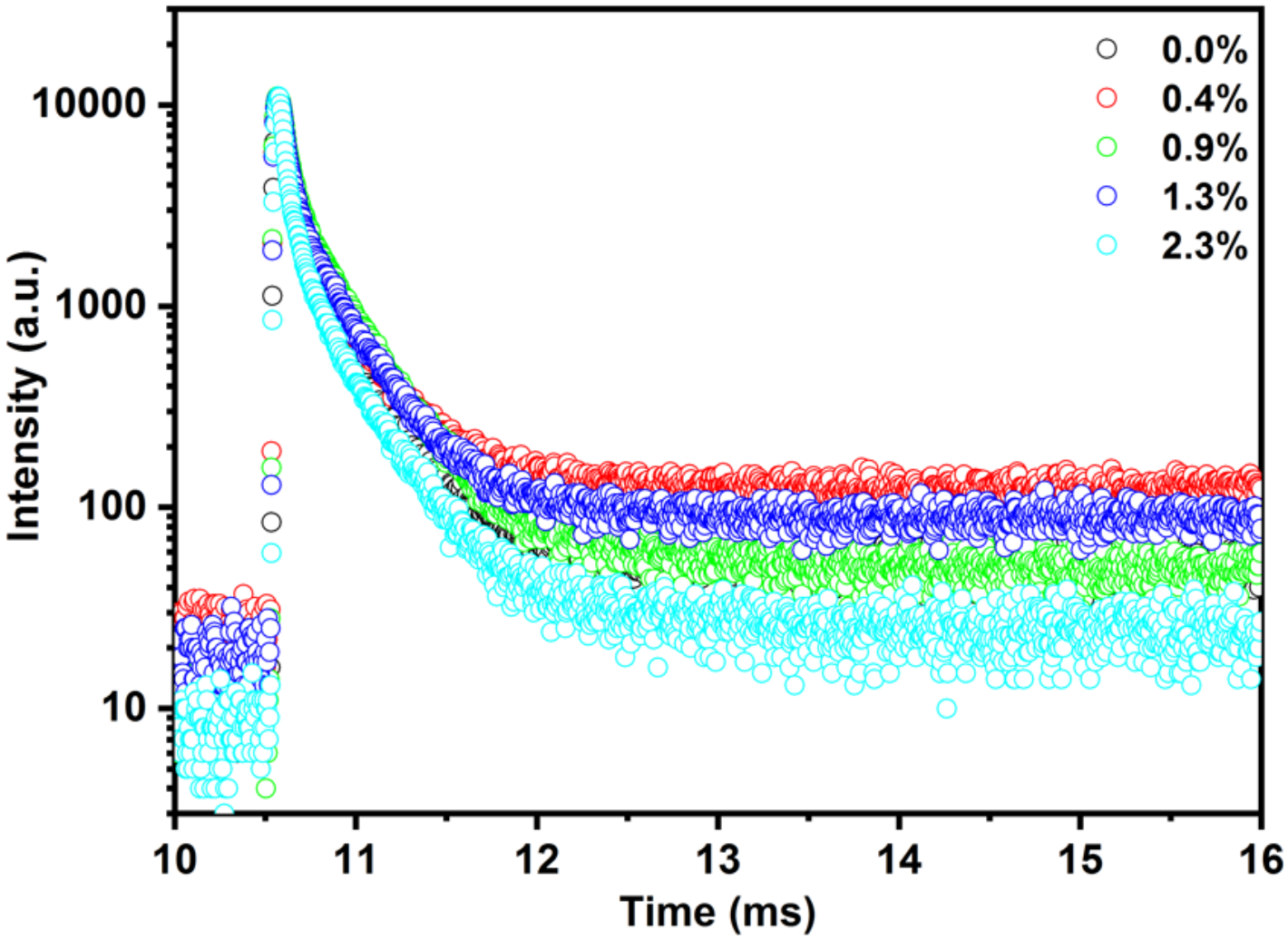

Figure 9

Decay curves under excitation of 266 nm and monitored at 597 nm of AlN: xMn nanowires

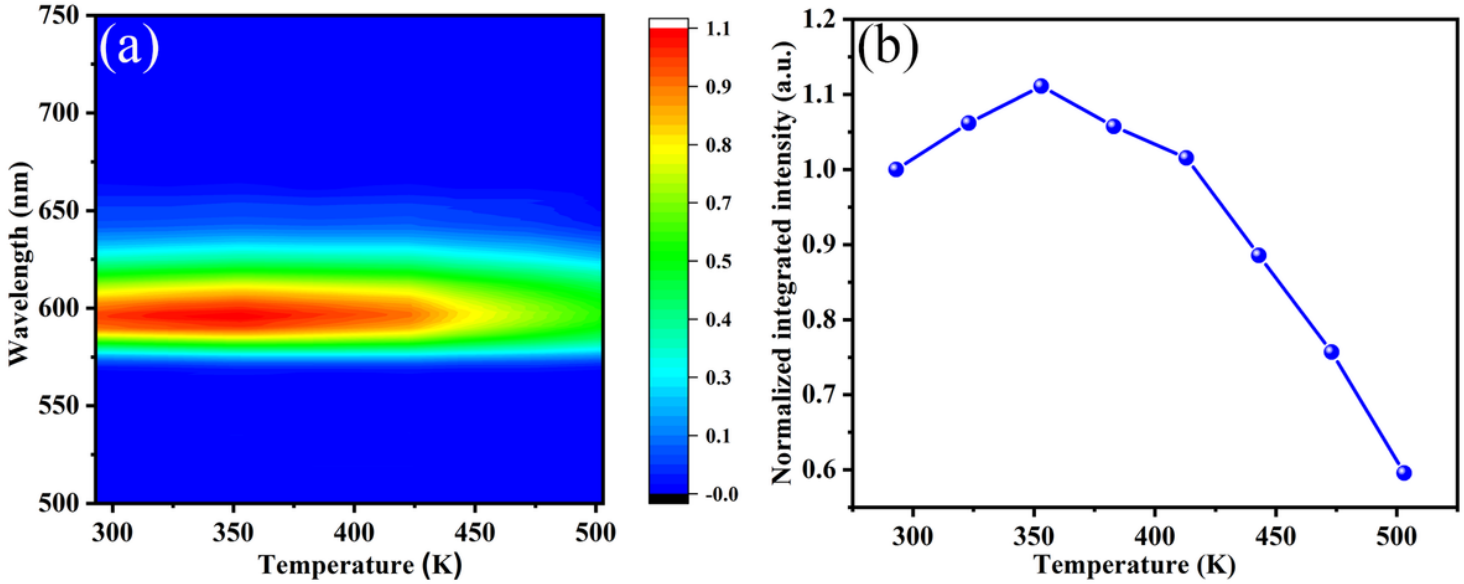

Figure 10

(a) Thermal quenching behavior of emission spectra for AlN: 0.9 % Mn nanowires. (b) The normalized integrated intensity as a function of temperature.

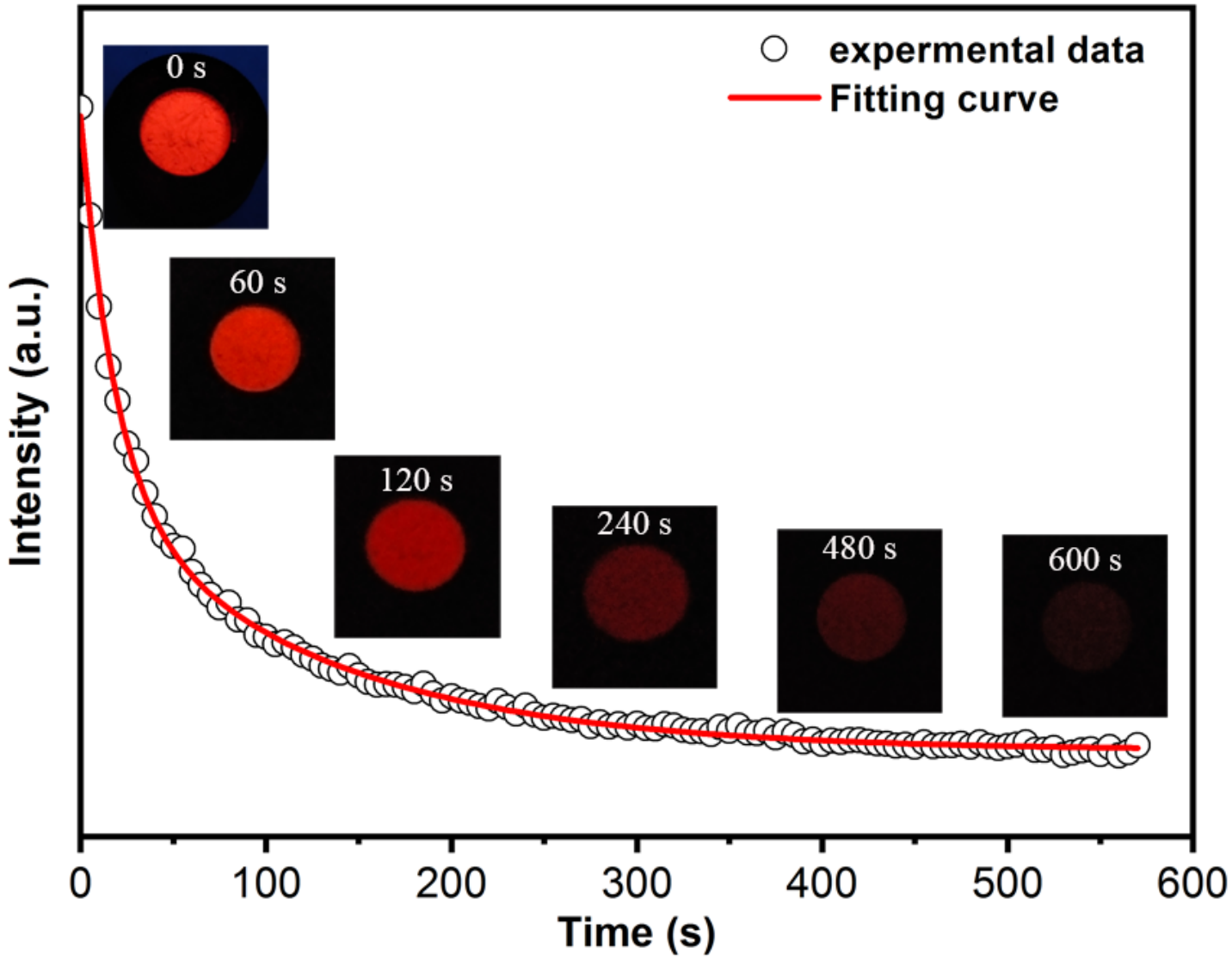

Figure 11

Afterglow decay curve of the AlN: Mn nanowires after excited by 254 nm light for 3 min. The inset shows optical images taken at different decay times after removal of the excitation source.

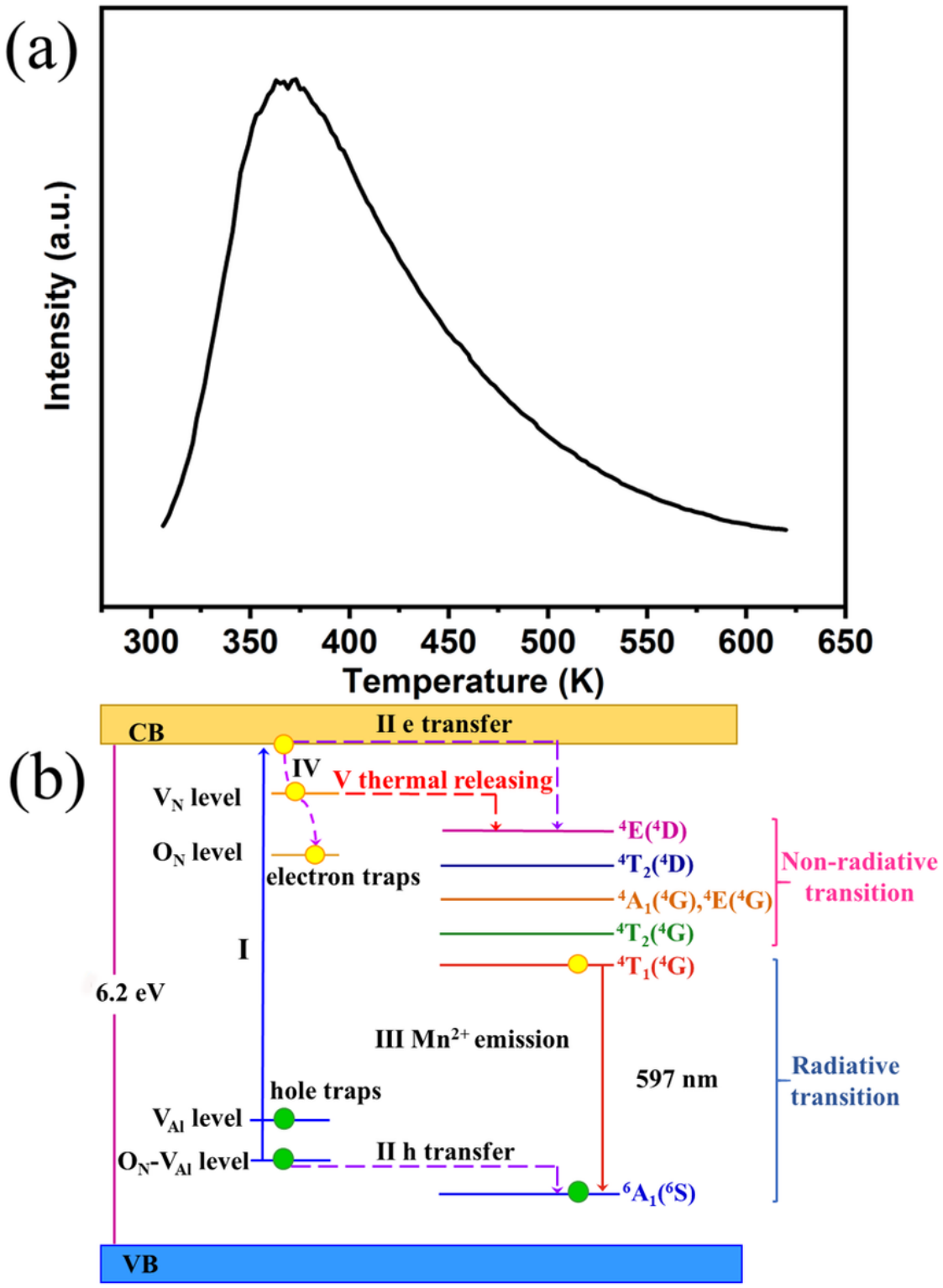

Figure 12

(a) The thermoluminescence curve of AlN: 0.9 % Mn nanowires and (d) Schematic illustration of the long afterglow mechanism and abnormal thermal behavior in AlN: 0.9 % Mn nanowires.